Longitudinal pressure-driven flows between superhydrophobic grooved surfaces: large effective slip in the narrow-channel limit

Ory Schnitzer

Department of Mathematics, Imperial College London,

South Kensington Campus, SW7 2AZ, London, United Kingdom

Ehud Yariv

Department of Mathematics, Technion — Israel Institute of Technology, Haifa 32000, Israel

(Dated: June 21, 2017)

Abstract

The gross amplification of the fluid velocity in pressure-driven flows due to the introduction of superhydrophobic walls is commonly quantified by an effective slip length. The canonical duct-flow geometry involves a periodic structure of longitudinal shear-free stripes at either one or both of the bounding walls, corresponding to flat-meniscus gas bubbles trapped within a periodic array of grooves. This grating configuration is characterized by two geometric parameters, namely the ratio κ of channel width to microstructure period and the areal fraction Δ of the shear-free stripes. For wide channels, $\kappa \gg 1$, this geometry is known to possess an approximate solution where the dimensionless slip length λ, normalized by the duct semi-width, is small, indicating a weak superhydrophobic effect. We here address the other extreme of narrow channels, $\kappa \ll 1$, identifying large $O(\kappa^{-2})$ values of λ for the symmetric configuration, where both bounding walls are superhydrophobic. This velocity enhancement is associated with an unconventional Poiseuille-like flow profile where the parabolic velocity variation takes place in a direction parallel (rather than perpendicular) to the boundaries. Use of matched asymptotic expansions and conformal-mapping techniques provides λ up to $O(\kappa^{-1})$, establishing the approximation

$$\lambda \sim \kappa^{-2}\frac{\Delta^3}{3} + \kappa^{-1}\frac{\Delta^2}{\pi}\ln 4 + \cdots ,$$

which is in excellent agreement with a semi-analytic solution of the dual equations governing the respective coefficients of a Fourier-series representation of the fluid velocity. No similar singularity occurs in the corresponding asymmetric configuration, where only one of the bounding walls is superhydrophobic; in that geometry, a Hele-Shaw approximation shows that $\lambda = O(1)$.

I. INTRODUCTION

The viscous resistance to fluid motion in micro-channels necessitates the application of large pressure heads. There exists accordingly significant interest in the possibility of reducing viscous friction over solid surfaces. One of the promising directions involves the use of superhydrophobic surfaces, namely solid surfaces which are deliberately patterned with a periodic microstructure. With gas bubbles trapped in a Cassie state within the microstructure pockets, the overall resistance to flow may be reduced compared to that about a homogeneous solid boundary. A common measure of drag reduction in channel flows, employed in both experimental [1, 2] and theoretical [3–5] work, is the effective slip length. It is defined as the slip length appearing in a Navier-type condition which, when applied over a hypothetical homogeneous boundary, would predict the same volumetric flux.

The first experimental illustration of superhydrophobic effects due to deliberate patterning was carried out by Ou *et al.* [6] who investigated pressure-driven flows in microchannels of rectangular cross section, where the superhydrophobic microstructure consists of a series of gas-filled grooves aligned with the flow. This "longitudinal" duct geometry has since become the preferred mode in experimental setups [1, 6, 7]. Longitudinal problems are also convenient for analysis, since the fully-developed flow is unidirectional, with the pressure varying linearly with the longitudinal coordinate and the fluid velocity being independent of that coordinate. The velocity dependence upon the cross-sectional coordinates is therefore governed by a Poisson equation for any value of the Reynolds number for which the flow is laminar.

When the number of grooves is large the duct configuration may be modeled by infinite planar surfaces which are decorated with periodic arrays of grooves. The simplest geometry involves bubbles of flat menisci; the cross-sectional channel geometry is then described by two parameters: the first is the ratio κ of the channel width to microstructure period, and the second is the no-shear fraction Δ (namely the ratio of the groove length to that period). The dependence of the dimensionless slip length λ, normalized by the channel semi-width, upon these two parameters constitutes a lumped description of the channel superhydrophobicity. The first theoretical analysis of longitudinal flow in this type of geometry [8] was carried out by Sbragaglia & Prosperetti [4]. Motivated by the specific experiments of Ou *et al.* [6, 7], Sbragaglia & Prosperetti [4] considered an asymmetric configuration; thus, while the bottom channel wall was assumed to be patterned with a periodic array of longitudinal no-shear stripes, the upper wall was assumed homogeneous. While the associated mixed boundary-condition problem has already been solved in closed form by Philip [9] using conformal maps, that solution is expressed in terms of cumbersome Jacobian elliptic functions. Sbragaglia & Prosperetti [4] have accordingly introduced Fourier-series expansions, solving the resulting dual series equations numerically. The corresponding symmetric configuration, where longitudinal no-shear stripes are prescribed at the two channel walls, was analyzed by Teo & Khoo [5]. Similarly to Ref. 4, this problem was handled using Fourier-series expansions. (This symmetric configuration has not been solved in Ref. 9.)

It is of interest to supplement the above exact solutions with asymptotic approximations. For wide channels, where $\kappa \gg 1$, each compound surface is effectively exposed to a homogeneous shear. Making use of Philip's solution of the corresponding unbounded problem [9] then gives for the symmetric configuration [10],

$$\lambda \sim \frac{2}{\pi\kappa} \ln \sec \frac{\pi\Delta}{2} \quad \text{for} \quad \kappa \gg 1, \tag{1}$$

and half of that for the asymmetric configuration (in agreement with Ref. 4). Unsurprisingly, the slip length turns out asymptotically small, representing a weak effect. Our interest is in the other extreme of narrow channels, $\kappa \ll 1$, a geometric limit which has already attracted some attention in the superhydrophobic literature [11, 12].

In particular, we focus upon the symmetric configuration, where Teo & Khoo [5] have observed large superhydrophobic effect for small numerical values of κ — a phenomenon which has no counterpart in the asymmetric configuration. Being unable to provide an asymptotic approximation for the large slip length, Teo & Khoo [5] have proposed instead an empirical correlation involving a κ^{-2}-like divergence of λ. With the goal of illuminating this slip-length singularity and providing a systematic approximation for the sip length, we here address the narrow-channel limit using singular perturbations.

II. PROBLEM FORMULATION

We consider pressure-driven liquid flow between two parallel micro-structured interfaces, separated a distance $2h$ apart. The microstructure is formed by an infinite array of grooves at each boundary, where air bubbles are trapped in the Cassie state, pinned at the solid corners.

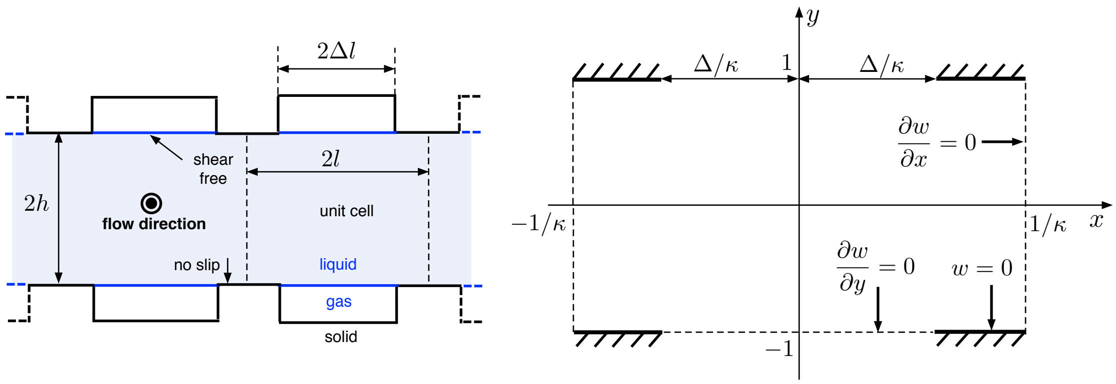

FIG. 1. (a) Schematic of the dimensional channel geometry; (b) Schematic of the dimensionless unit-cell geometry.

Denoting the microstructure period by $2l$ and assuming flat free surfaces, each interface is accordingly compound of a periodic array of solid segments, say of length $2(1-\Delta)l$, and free surfaces of length $2\Delta l$. The dimensional geometry is depicted in Fig. 1(a).

A uniform pressure-gradient G is applied parallel to the grooves, resulting in a unidirectional flow anti-parallel to the gradient. The associated two-dimensional fluid domain is naturally decomposed into an infinite array of rectangular cells of width $2h$ and length $2l$. Using h as a unit of measure we define Cartesian coordinates (x, y) with the lines $y = \pm 1$ coinciding with the compound boundaries and the symmetry line $x = 0$ bisecting two opposite free surfaces, see Fig. 1(b). The associated z-direction is anti-parallel to the pressure gradient. Because of periodicity it is sufficient to consider the flow in a single cell, say that containing the origin. The fluid domain is accordingly is bounded by the periodic boundaries $x = \pm 1/\kappa$, where $\kappa = h/l$ is the channel narrowness, and the two boundaries $y = \pm 1$; each of these consists of a free surface, extending between $-\Delta/\kappa < x < \Delta/\kappa$, and two solid segments of length $(1-\Delta)/\kappa$.

We normalize the z-component w of the fluid velocity by Gh^2/μ, μ being the liquid viscosity. The function $w(x, y)$ is governed by Poisson's equation,

$$\frac{\partial^2 w}{\partial x^2} + \frac{\partial^2 w}{\partial y^2} = -1 \quad \text{for} \quad -\frac{1}{\kappa} < x < \frac{1}{\kappa}, \quad -1 < y < 1. \tag{2}$$

At $y = \pm 1$ w satisfies a mixed condition, consisting of a shear-free condition at the free surfaces,

$$\frac{\partial w}{\partial y} = 0 \quad \text{at} \quad |x| < \frac{\Delta}{\kappa}, \tag{3}$$

and a no-slip condition at the solid segments

$$w = 0 \quad \text{for} \quad \frac{\Delta}{\kappa} < |x| < \frac{1}{\kappa}. \tag{4}$$

In addition, it satisfies a periodicity condition at $x = \pm 1/\kappa$. Given the obvious symmetry about $x = 0$ this condition is equivalent to the homogenous Neumann conditions,

$$\frac{\partial w}{\partial x} = 0 \quad \text{at} \quad x = \pm\frac{1}{\kappa}. \tag{5}$$

Our interest is not in the detailed function $w(x, y)$ but rather in the lumped measure of superhydrophobicity. A natural measure is the mean velocity, namely the net volumetric flux through the cell divided by its area, $4/\kappa$:

$$\bar{w} = \frac{\kappa}{4}\int_{-1/\kappa}^{1/\kappa} dx \int_{-1}^{1} dy\, w. \tag{6}$$

It is common to represent $\bar{w}$ via an effective slip length. Thus, the fictitious flow due to a homogenous Navier condition,

$$w = \mp\lambda\frac{\partial w}{\partial y} \quad \text{at} \quad y = \pm 1, \tag{7}$$

is $w = (1 - y^2)/2 + \lambda$, where the associated mean velocity is $\lambda + 1/3$. The dimensionless slip length λ is obtained by equating the real and fictitious fluxes (or, equivalently, mean velocities), giving

$$\lambda = \bar{w} - \frac{1}{3}. \tag{8}$$

III. SEMI-ANALYTIC SOLUTION

As already mentioned, the slip length has been determined in the wide-channel limit $\kappa \gg 1$, giving the small value (1). Our interest here is in the other extreme of narrow channels, $\kappa \ll 1$. Before addressing this singular limit, we briefly describe the construction of a semi-analytic solution of the exact problem, following Teo & Khoo [5]. (See also Appendix C of Ref. 4.) We write

$$w = \frac{1 - y^2}{2} + \grave{w} \tag{9}$$

where $\grave{w}$ satisfies the homogeneous Neumann conditions (5) at $x = \pm 1$. Since $\grave{w}$ is harmonic, it is readily written as the following Fourier series,

$$\grave{w} = \sum_{n=0}^{\infty} A_n \cosh k_n y \cos k_n x, \tag{10}$$

where $k_n = n\pi\kappa$. Application of (3)–(4) gives:

$$\sum_{n=0}^{\infty} k_n A_n \sinh k_n \cos n\pi\theta = 1 \quad \text{for} \quad 0 < \theta < \Delta, \tag{11a}$$

$$\sum_{n=0}^{\infty} A_n \cosh k_n \cos n\pi\theta = 0 \quad \text{for} \quad \Delta < \theta < 1. \tag{11b}$$

Multiplication of (11a)–(11b) by $\cos m\pi\theta$ ($m = 0, 1, 2, \dots$) followed by integration over $0 < \theta < \Delta$ and $\Delta < \theta < 1$, respectively, yields two infinite system of algebraic equations governing the coefficients $\{A_n\}_{n=0}^{\infty}$. Mutual addition yields a dual linear equation, which is solved by controlled truncation. Once the coefficients are evaluated we obtain the dimensionless slip length $\lambda = A_0$, see (8)–(10). The resulting semi-analytic calculation is used below for comparison with the asymptotic approximation.

IV. NARROW-CHANNEL LIMIT

When considering the narrow-channel limit, $\kappa \ll 1$, it is natural to employ the rescaled longitudinal coordinate $\tilde{x} = \kappa x$. Poisson's equation (2) then becomes

$$\frac{\partial^2 w}{\partial y^2} + \kappa^2 \frac{\partial^2 w}{\partial \tilde{x}^2} = -1 \quad \text{for} \quad -1 < y < 1, \quad -1 < \tilde{x} < 1, \tag{12}$$

while conditions (3)–(4) respectively read, at $y = \pm 1$,

$$\frac{\partial w}{\partial y} = 0 \quad \text{for} \quad |\tilde{x}| < \Delta, \qquad w = 0 \quad \text{for} \quad \Delta < |\tilde{x}| < 1. \tag{13a, b}$$

Equation (12) appears to suggest that the leading-order approximation to w, say w_0, satisfies

$$\frac{\partial^2 w_0}{\partial y^2} = -1. \tag{14}$$

The solution of that equation which satisfies the implicit symmetry about $y = 0$ is

$$w_0 = A(\tilde{x}) - \frac{y^2}{2}. \tag{15}$$

This solution, however, cannot satisfy the Neumann condition (13a).

The preceding incompatibility indicates a singular problem which is handled here using matched asymptotic expansions. We conceptually decompose the fluid domain into three asymptotic regions: the free-boundary region, $|\tilde{x}| < \Delta$, the solid-boundary region, $\Delta < \tilde{x} < 1$, and a transition region about $x = \Delta/\kappa$, of $O(1)$ extent in x-direction. (Given the underlying symmetry about $x = 0$ we omit the corresponding negative-x complements of the latter two regions.)

A. Solid-boundary region, $\Delta < \tilde{x} < 1$

In this region we simply postulate

$$w = w_0(\tilde{x}, y) + \cdots . \tag{16}$$

At leading-order we obtain (15); application of the Dirichlet condition (13b) then gives $A = 1/2$.

B. Free-boundary region, $|\tilde{x}| < \Delta$

The incompatibility of (15) with (13a) suggests here a balance between slow longitudinal variations of a y-independent $O(\kappa^{-2})$ term with fast transverse variations of an $O(1)$ correction. We accordingly postulate the asymptotic expansion

$$w = \kappa^{-2} w_{-2}(\tilde{x}) + \kappa^{-1} w_{-1}(\tilde{x}) + w_0(\tilde{x}, y) + \kappa w_1(\tilde{x}, y) + \cdots . \tag{17}$$

At leading order we obtain from (12):

$$\frac{d^2 w_{-2}}{d\tilde{x}^2} + \frac{\partial^2 w_0}{\partial y^2} = -1. \tag{18}$$

Integration over y in conjunction with the Neumann condition (13a) yields

$$\frac{d^2 w_{-2}}{d\tilde{x}^2} = -1. \tag{19}$$

The solution of (19) that satisfies the symmetry about $x = 0$ is

$$w_{-2} = B - \frac{\tilde{x}^2}{2}, \tag{20}$$

representing an unconventional Poiseuille-like flow, where the parabolic variation takes place parallel to the boundary, rather then perpendicular to it.

C. Transition region, $x - \Delta/\kappa = O(1)$

Employing the shifted coordinate $s = x - \Delta/\kappa$, the transition-region domain is the infinite strip $\mathcal{D} = \{(s, y)| -\infty < s < \infty, -1 < y < 1\}$. Matching with the $O(\kappa^{-2})$ velocity in the free-boundary region suggests here the expansion

$$w = \kappa^{-2} W_{-2}(s, y) + \kappa^{-1} W_{-1}(s, y) + \cdots , \tag{21}$$

where W_{-2} satisfies

$$W_{-2} \to B - \frac{\Delta^2}{2} \quad \text{as} \quad s \to -\infty. \tag{22}$$

Note that W_{-2} is harmonic,

$$\frac{\partial^2 W_{-2}}{\partial s^2} + \frac{\partial^2 W_{-2}}{\partial y^2} = 0 \quad \text{in} \quad \mathcal{D}. \tag{23}$$

In addition to (22)–(23), W_{-2} also satisfies the mixed conditions at $y = \pm 1$ (cf. (3)–(4)),

$$\frac{\partial W_{-2}}{\partial y} = 0 \quad \text{for} \quad s < 0, \qquad W_{-2} = 0 \quad \text{for} \quad s > 0, \tag{24a, b}$$

and the decay condition,

$$W_{-2} \to 0 \quad \text{as} \quad s \to \infty, \tag{25}$$

which follows from matching with the $O(1)$ velocity in the solid-boundary region.

Since Laplace's equation in unbounded domains is typically incompatible with a transition from one uniform value at infinity to another, we assert that the preceding problem has a solution only if the limits attained as $s \to \pm\infty$ coincide, namely

$$B = \frac{\Delta^2}{2}. \tag{26}$$

Indeed, multiplying Laplace's equation (23) by W_{-2} and making use of Green's identity in a manner familiar from standard uniqueness proofs it is readily shown that $\boldsymbol{\nabla} W_{-2}$ vanishes, whereby (25) necessitates $W_{-2} \equiv 0$. Assertion (26) then follows from (22).

D. Leading-order flux

Having obtained B, the leading-order velocity (20) in the free-boundary region is fully determined. As this velocity is $O(\kappa^{-2})$, the mean velocity (6) possesses the expansion

$$\bar{w} = \kappa^{-2}\bar{w}_{-2} + \kappa^{-1}\bar{w}_{-1} + \cdots , \tag{27}$$

where the leading-order term is contributed solely by the free-boundary region,

$$\bar{w}_{-2} = \frac{1}{4}\int_{-\Delta}^{\Delta} d\tilde{x} \int_{-1}^{1} dy \, w_{-2}. \tag{28}$$

Substitution of (20) and (26) gives $\bar{w}_{-2} = \Delta^3/3$.

E. Leading-order correction

The preceding asymptotic matching reveals that the presumably leading-order term in the transition-region expansion (21) trivially vanishes. Nonetheless, the non-vanishing of $dw_{-2}/d\tilde{x}$ at $\tilde{x} = \Delta$ necessitates an $O(\kappa^{-1})$ term in that expansion. While the contribution of that term to the mean velocity (6) is merely $O(1)$, it triggers an $O(\kappa^{-1})$ velocity in the free-boundary region which gives rise to an $O(\kappa^{-1})$ contribution to $\bar{w}$.

We accordingly proceed with the calculation of W_{-1} which, just like W_{-2}, is governed by Laplace's equation, the homogeneous conditions at $y = \pm 1$,

$$\frac{\partial W_{-1}}{\partial y} = 0 \quad \text{for} \quad s < 0, \qquad W_{-1} = 0 \quad \text{for} \quad s > 0, \tag{29a, b}$$

and the large-s decay

$$W_{-1} \to 0 \quad \text{as} \quad s \to \infty, \tag{30}$$

which follows from the $O(1)$ magnitude of the velocity in the solid-boundary region. In contrast to W_{-2}, however, W_{-1} satisfies the flux condition,

$$\frac{\partial W_{-1}}{\partial s} \to -\Delta \quad \text{as} \quad s \to -\infty, \tag{31}$$

which follows from longitudinal-derivative matching with the free-boundary region. This implies the algebraic divergence

$$W_{-1} \sim -s\Delta \quad \text{as} \quad s \to -\infty, \tag{32}$$

which constitutes the leading-order term in an asymptotic expansion.

Our interest is not in the details of W_{-1} but rather in the $O(1)$ "displacement"-like correction to (32). In the Appendix we analyze the above boundary-value problem governing W_{-1}, showing that (32) is refined to

$$W_{-1} \sim -\left[s + \frac{\ln 4}{\pi} + o(1)\right]\Delta \quad \text{as} \quad s \to -\infty. \tag{33}$$

With the $O(1)$ term determined we proceed to the evaluation of w_{-1} in the free-boundary region. At $O(\kappa^{-1})$, Poisson's equation (12) yields there:

$$\frac{d^2 w_{-1}}{d\tilde{x}^2} + \frac{\partial^2 w_1}{\partial y^2} = 0. \tag{34}$$

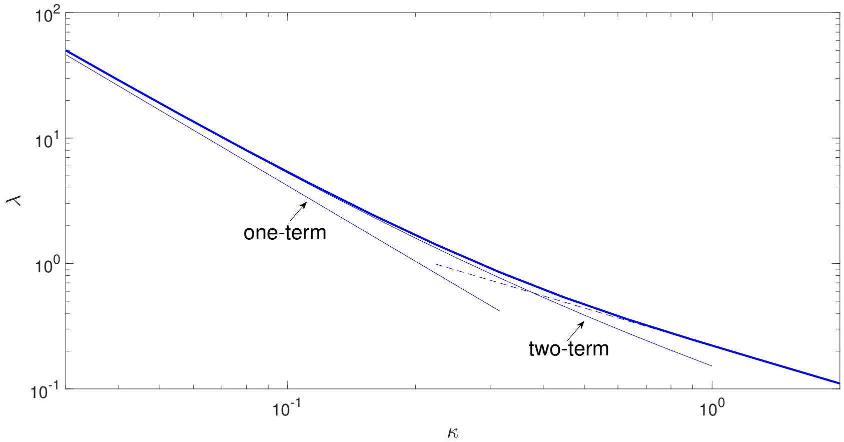

FIG. 2. λ as a function of κ for $\Delta = 1/2$. The thick line depicts the semi-analytic solution, while the thin lines respectively depict the one-term approximation $\kappa^{-2}\Delta^3/3$ and the two-term approximation (37) for narrow channels. Also shown (dashed) is the wide-channel approximation (1).

Integration over y in conjunction with the Neumann condition ($13a$) yields $d^2w_{-1}/d\tilde{x}^2 = 0$; given the symmetry about $x = 0$ we conclude that w_{-1} is a constant. Asymptotic matching with (31) thus gives

$$w_{-1} \equiv \frac{\Delta}{\pi}\ln 4. \tag{35}$$

Just as $\bar{w}_{-2}$, its leading-order correction is contributed solely by the free-boundary region

$$\bar{w}_{-1} = \frac{1}{4}\int_{-\Delta}^{\Delta} d\tilde{x}\int_{-1}^{1} dy\, w_{-1}; \tag{36}$$

since w_{-1} is uniform, this gives $\bar{w}_{-1} = w_{-1}\Delta$. At the present level of approximation, (8) gives a dimensionless slip length which is identical to the mean velocity, namely

$$\lambda \sim \kappa^{-2}\frac{\Delta^3}{3} + \kappa^{-1}\frac{\Delta^2}{\pi}\ln 4 + \cdots . \tag{37}$$

V. CONCLUDING REMARKS

Our analysis quantifies and illuminates the physics underlying the large $O(\kappa^{-2})$ slip length observed for longitudinal pressure driven flow through symmetric narrow channels. On the quantitative side, our asymptotic formula (37) provides an accurate two-term approximation for the effective slip length in the limit of narrow channels. In Fig. 2 we compare the one-term and two-term versions of this approximation with the semi-analytic solution of Sec. III. The agreement is gratifying. Also shown is the wide-channel approximation (1). Taken together, the disjoint approximations (1) and (37) practically provide useful formulae for λ over the entire range of κ.

It is useful to recap in dimensional terms the basic mechanism enabling the large effective slip. The key idea is that the pressure force exerted on a volume of liquid bounded between two opposing gaseous shear-free patches can only be balanced by viscous shear stresses, with the pertinent velocity gradients being set by the need to continuously merge with the relatively slow flow of liquid in the adjacent solid-boundary regions. On the one hand, the magnitude of the pressure force per unit length is $O(Glh)$. On the other hand, we have seen that the narrowness of the channels implies that in the free-boundary regions the flow is approximately uniform across the channel, varying according to a Poiseuille-like profile over $O(l)$ distances in a direction parallel to the periodicity. Thus, by balancing the pressure and shear-stress forces we see that the velocity in the free-boundary regions scales as $O(Gl^2/\mu)$, signifying an $O(l^2/h^2)$ enhancement relative to the conventional scaling for pressure-driven velocity holding in the solid-boundary portions.

Our asymptotic analysis may also serve to explain why no comparable enhancement occurs for the asymmetric configuration. Indeed, making use of the present decomposition of the fluid domain, now with the free-boundary region becoming a "mixed-boundary" region, it is evident that (14) is consistent with the boundary conditions in *both* the mixed- and solid-boundary regions. A straightforward analysis then reveals that the cross-sectional velocity average in the mixed-boundary region, $4/3$, is merely four times that in the solid-boundary region. The dimensionless slip length is accordingly $O(1)$.

The fundamental difference between the asymmetric and symmetric configurations sheds light on the applicability of a Hele-Shaw description to narrow channels. The approximate balance underlying that description, between shear across the channel and pressure gradients along it, gives rise to a the permeability concept. In the asymmetric geometry that balance indeed holds (see (14)); its violation in the transition region represents a mere local breakdown. In the symmetric problem, on the other hand, that balance is violated globally in the free-boundary region, where it is the shear along the channel that balances the pressure gradient (see (19)). An averaging scheme based upon the Hele-Shaw approximation is

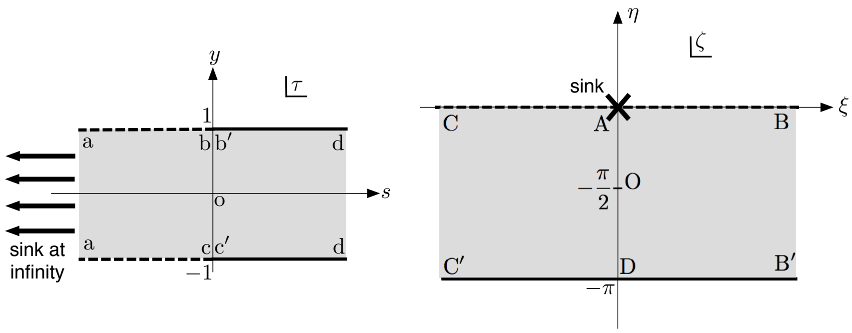

FIG. 3. Illustration of the mapping from the infinite strip $\mathcal{D}$ in the complex τ-plane to the infinite strip $-\pi < \mathrm{Im}\{\zeta\} < 0$, affected by (A.1). The solid and dashed boundaries respectively represent homogeneous Dirichlet and Neumann conditions.

accordingly inapplicable to that geometry. Such an scheme was constructed by Feuillebois *et al.* [12] for arbitrary geometries, where the slippery patches at the boundary were modeled using a local Navier slip condition. In adapting that condition to accommodate free surfaces, the slip length appearing therein is set to infinity. It is readily verified that the Hele-Shaw permeability in [12] (see (2) there) then becomes unbounded for the symmetric configuration addressed in the present paper.

A natural followup of the present analysis has to do with the other singular limit of small solid fractions, $\Delta \to 1$ [13]. By forming the appropriate limits of their pertinent exact solution, Teo & Khoo [5] have claimed to find a $(1-\Delta)^{-1}$-type singularity of the slip length. This strong singularity appears to be at odds with our semi-analytic solution. Understanding the underlying mechanism in that singular limit requires a companion asymptotic investigation, following earlier analyses in unbounded shear flows [14, 15].

Appendix: Derivation of (33)

We regard the harmonic function W_{-1} as the real part of $F\Delta$, F being an analytic function of $\tau = s + iy$ in the infinite strip $\mathcal{D}$. We define $\zeta = f(\tau)$ with $\zeta = \xi + i\eta$ and

$$f(\tau) = \log\left\{\tanh\frac{\pi(\tau+i)}{4}\right\} - i\pi, \tag{A.1}$$

in which the principal branch of the logarithm is employed. The function f maps $\mathcal{D}$ onto the infinite trip $-\pi < \mathrm{Im}\{\zeta\} < 0$, see Fig. 3.

We seek an analytic function $\Phi(\zeta)$ such that $F(\tau) = \Phi(f(\tau))$. Following the theory of conformal mappings, the real part of Φ, say $\varphi(\xi, \eta)$, must satisfy a homogeneous Dirichlet condition at the image of the no-slip boundaries of $\mathcal{D}$,

$$\varphi = 0 \quad \text{at} \quad \eta = -\pi, \tag{A.2}$$

and a homogeneous Neumann condition at the image of the no-shear boundaries,

$$\frac{\partial \varphi}{\partial \eta} = 0 \quad \text{at} \quad \eta = 0. \tag{A.3}$$

In addition, φ must properly represent the algebraic divergence of W_{-1} at $\tau = \infty$ (with $\operatorname{Re}\{\tau\} \to -\infty$); since condition (31) amounts to a sink of magnitude 2 there, and with that infinity mapped to the origin of the ζ plane, we need a point sink of magnitude 4 at $\zeta = 0$:

$$\varphi \sim -\frac{2}{\pi} \ln \sqrt{\xi^2 + \eta^2} \quad \text{as} \quad \xi^2 + \eta^2 \to 0. \tag{A.4}$$

As our goal lies in the refinement of (32) we need the behavior of φ near the origin singularity.

Given the homogeneous Neumann condition (A.3), the problem governing φ is conveniently analyzed by forming an even extension about $\eta = 0$; condition (A.2) thus becomes

$$\varphi = 0 \quad \text{at} \quad \eta = \pm\pi. \tag{A.5}$$

In addition, we note that the sink singularity (A.4) may be represented as a Dirac forcing term in Laplace's equation governing φ:

$$\frac{\partial^2 \varphi}{\partial \xi^2} + \frac{\partial^2 \varphi}{\partial \eta^2} = -4\delta(\xi)\delta(\eta). \tag{A.6}$$

Application of a Fourier transform in ξ to the problem (A.5)–(A.6) followed by inversion and substitution of $\eta = 0$ yields

$$\varphi(\xi, 0) = \frac{1}{\pi} \int_{-\infty}^{\infty} \frac{\tanh \pi k}{k} e^{-ik\xi}\, dk. \tag{A.7}$$

Our goal in to obtain an asymptotic expansion of this integral for small (say positive) ξ. Defining the auxiliary variable $1 \ll \Lambda \ll 1/\xi$ we split the integral [16]:

$$\varphi(\xi, 0) = \frac{1}{\pi} \left(\int_{-\infty}^{-\Lambda} + \int_{-\Lambda}^{\Lambda} + \int_{\Lambda}^{\infty} \right) \frac{\tanh \pi k}{k} e^{-ik\xi}\, dk. \tag{A.8}$$

In the first and third integrals (the "global" contribution), where k is large, $\tanh \pi k$ is respectively approximated by ∓ 1, giving

$$\left(\int_{\Lambda}^{\infty} - \int_{-\infty}^{-\Lambda} \right) \frac{e^{-ik\xi}}{k}\, dk \sim 2\left(\ln \frac{1}{\Lambda \xi} - \gamma \right) + o(1) \quad \text{as} \quad \xi \to 0, \tag{A.9}$$

where γ is the Euler–Mascheroni constant. In the second ("local") integral of (A.8), where $k\xi$ is small, $e^{-ik\xi} \sim 1$. We conclude that

$$\varphi(\xi, 0) \sim \frac{2}{\pi}\left[\ln\frac{1}{\xi} + C + o(1)\right] \quad \text{as} \quad \xi \to 0, \tag{A.10}$$

where

$$C = -\gamma + \lim_{\Lambda\to\infty}\left(\int_0^\Lambda \frac{\tanh \pi k}{k}\, dk - \ln\Lambda\right). \tag{A.11}$$

To calculate the above limit we employ the asymptotic expansion

$$\int_0^\Lambda \frac{1-e^{-k}}{k}\, dk \sim \ln\Lambda + \gamma + o(1) \quad \text{as} \quad \Lambda \to \infty, \tag{A.12}$$

where the integrand possesses the same slow $1/k$ decay as that in (A.11). We find

$$C = \int_0^\infty \frac{\tanh \pi k - 1 + e^{-k}}{k}\, dk = \ln 4. \tag{A.13}$$

Given (A.10), expansion (A.4) is modified to

$$\varphi \sim -\frac{2}{\pi}\left[\ln\sqrt{\xi^2+\eta^2} - \ln 4 + o(1)\right] \quad \text{as} \quad \xi^2+\eta^2 \to 0, \tag{A.14}$$

implying the comparable expansion of the complex potential

$$\Phi(\zeta) \sim -\frac{2}{\pi}\left[\log(\zeta/4) + \text{purely imaginary constant} + o(1)\right] \quad \text{as} \quad \zeta \to 0. \tag{A.15}$$

As $s \to -\infty$ we find from (A.1)

$$\zeta \sim -2e^{\pi(\tau+i)/2} \tag{A.16}$$

with an exponentially small error. Substituting into (A.15) and forming the real part yields (33).

[1] P. Tsai, A. M. Peters, C. Pirat, M. Wessling, R. G. H. Lammertink, and D. Lohse, "Quantifying effective slip length over micropatterned hydrophobic surfaces," Phys. Fluids **21**, 112002 (2009).

[2] E. Karatay, A. S. Haase, C. W. Visser, C. Sun, D. Lohse, P. A. Tsai, and R. G. H. Lammertink, "Control of slippage with tunable bubble mattresses," Proc. Natl. Acad. Sci. U.S.A. **110**, 8422–8426 (2013).

[3] E. Lauga and H. A. Stone, "Effective slip in pressure-driven Stokes flow," J. Fluid Mech **489**, 55–77 (2003).

[4] M. Sbragaglia and A. Prosperetti, "A note on the effective slip properties for microchannel flows with ultrahydrophobic surfaces," Phys. Fluids **19**, 043603 (2007).

[5] C. J. Teo and B. C. Khoo, "Analysis of Stokes flow in microchannels with superhydrophobic surfaces containing a periodic array of micro-grooves," Microfluid. Nanofluid. **7**, 353–382 (2009).

[6] J. Ou, B. Perot, and J. P. Rothstein, "Laminar drag reduction in microchannels using ultrahydrophobic surfaces," Phys. Fluids **16**, 4635–4643 (2004).

[7] J. Ou and J. P. Rothstein, "Direct velocity measurements of the flow past drag-reducing ultrahydrophobic surfaces," Phys. Fluids **17**, 103606–11 (2005).

[8] The analysis in Ref. 4 actually allows for small defamation of the bubble menisci. The leading-order analysis in that paper accordingly involves flat menisci.

[9] J. R. Philip, "Flows satisfying mixed no-slip and no-shear conditions," Z. Angew. Math. Phys. **23**, 353–372 (1972).

[10] T. L. Kirk, M. Hodes, and D. T. Papageorgiou, "Nusselt numbers for Poiseuille flow over isoflux parallel ridges accounting for meniscus curvature," J. Fluid Mech. **811**, 315–349 (2017).

[11] O. I. Vinogradova, "Drainage of a thin liquid film confined between hydrophobic surfaces," Langmuir **11**, 2213–2220 (1995).

[12] F. Feuillebois, M. Z. Bazant, and O. I. Vinogradova, "Effective slip over superhydrophobic surfaces in thin channels," Phys. Rev. Lett. **102**, 026001 (2009).

[13] That singularity is not indicated by approximation (37). This is consistent with the implicit assumption $1 - \Delta = O(1)$ underlying our asymptotic analysis.

[14] O. Schnitzer, "Singular effective slip length for longitudinal flow over a dense bubble mattress," Phys. Rev. Fluids **1**, 052101 (2016).

[15] O. Schnitzer, "Slip length for longitudinal shear flow over an arbitrary-protrusion-angle bubble mattress: the small-solid-fraction singularity," J. Fluid Mech. **820**, 580–603 (2017).

[16] E. J. Hinch, *Perturbation Methods* (Cambridge University Press, Cambridge, 1991).